Biophysical Chemistry 156 (2011) 43–50

Contents lists available at ScienceDirect

Biophysical Chemistry

journal homepage: http://www.elsevier.com/locate/biophyschem

Comparing the structural properties of human and rat islet amyloid polypeptide by MD computer simulations

Maximilian N. Andrews, Roland Winter *

Faculty of Chemistry, Physical Chemistry I—Biophysical Chemistry, TU Dortmund University, D-44227 Dortmund, Germany

ARTICLE INFO

Article history:
Received 21 November 2010
Received in revised form 26 December 2010
Accepted 26 December 2010
Available online 31 December 2010

Keywords:
hIAPP
rIAPP
MD simulation
Disulfide bond
Proline

ABSTRACT

Conformational properties of the full-length human and rat islet amyloid polypeptide 1–37 (amyloidogenic hIAPP and non-amyloidogenic rIAPP, respectively) were studied at 310 and 330 K by MD simulations both for the cysteine (reduced IAPP) and cystine (oxidized IAPP) moieties. At all temperatures studied, IAPP does not adopt a well-defined conformation and is essentially random coil in solution, although transient helices appear forming along the peptide between residues 8 and 22, particularly in the reduced form. Above the water percolation transition (at 320 K), the reduced hIAPP moiety presents a considerably diminished helical content remaining unstructured, while the natural cystine moiety reaches a rather compact state, presenting a radius of gyration that is almost 10% smaller and characterized by intrapeptide H-bonds that form many β-bridges in the C-terminal region. This compact conformation presents a short end-to-end distance and seems to form through the formation of β-sheet conformations in the C-terminal region with a minimization of the Y/F distances in a two-step mechanism: the first step taking place when the Y37/F23 distance is ~1.1 nm, and subsequently Y37/F15 reaches its minimum of ~0.86 nm. rIAPP, which does not aggregate, also presents transient helical conformations. A particularly stable helix is located in proximity of the C-terminal region, starting from residues L27 and P28. Our MD simulations show that P28 in rIAPP influences the secondary structure of IAPP by stabilizing the peptide in helical conformations. When this helix is not present, the peptide presents bends or H-bonded turns at P28 that seem to inhibit the formation of the β-bridges seen in hIAPP. Conversely, hIAPP is highly disordered in the C-terminal region, presenting transient isolated β-strand conformations, particularly at higher temperatures and when the natural disulfide bond is present. Such conformational differences found in our simulations could be responsible for the different aggregational propensities of the two different homologues. In fact, the fragment 30–37, which is identical in both homologues, is known to aggregate *in vitro*, hence the overall sequence must be responsible for the amyloidogenicity of hIAPP. The increased helicity in rIAPP induced by the serine-to-proline variation at residue 28 seems to be a plausible inhibitor of its aggregation.

1. Introduction

Many degenerative diseases, like Alzheimer's, Parkinson's, Creutzfeldt–Jakob, Diabetes Mellitus type II, and several other systematic amyloidoses are related to polypeptide aggregation. Human amyloid polypeptide (hIAPP) forms pancreatic amyloid deposits, which are found in more than 95% of the type II diabetes patients, although the causal relationship between amyloid formation and the disease is still largely unknown [1–4]. In aqueous solution, hIAPP has been shown to have an essentially disordered conformation as seen in far UV-CD [5–9]. However, it may also assume compact structures [8] and a transient sampling of α-helical conformations has been observed [11,12]. The former has been proven through FRET and the latter through NMR spectroscopic studies. The Förster distance between tyrosine and phenylalanine measured for hIAPP in the lag phase of the aggregation process is 12.6 Å, which, if compared to the values obtained through a random walk model [12], *i.e.*, 30 Å for Y37/F23 and 40 Å for Y37/F15, clearly reveals a structure that is more compact than what is expected for a fully unfolded peptide. The two homologues, human and rat IAPP, when free in solution, show comparable structures; in fact rIAPP adopts structures which are similar to hIAPP prefibrillar states [8]. Other studies reveal sampling of α-helical conformations in the central region of the peptide for about 40% of its length, starting approximately after the tight disulfide bond. The NMR chemical shifts indicate α-helical propensity from residues 5–19 and their temperature coefficients indicate such a region from residues 7 to 22. Therefore, the first fraction (residues 1–20) of both hIAPP and rIAPP seems to have a modest helical propensity, while the remaining fraction of the peptide (residues 21–37) seems to be less structured. Moreover, such helicity seems to be required for the biologically active state [10]. The sequences of hIAPP and rIAPP are 84% identical, and with the exception of residue 18, the different residues are localized between 20

* Corresponding author.
E-mail addresses: maximilian.andrews@tu-dortmund.de (M.N. Andrews), roland.winter@tu-dortmund.de (R. Winter).

0301-4622/$ – see front matter © 2011 Elsevier B.V. All rights reserved.
doi:10.1016/j.bpc.2010.12.007

and 29, which has been proven to be amyloidogenic in human and in cat. The primary structures of hIAPP and rIAPP are as follows:

```
      1         10         20         30
hIAPP KCNTATCAT QRLANFLVHS SNNFGAILSS TNVGSNTY-NH2
rIAPP KCNTATCAT QRLANFLVRS SNNLGPVLPP TNVGSNTY-NH2
```

where the most noticeable difference between hIAPP and rIAPP is the presence of proline in positions 25, 28 and 29 (in red) in rIAPP. Moreover, residue 23 (also in red) in rIAPP replaces an aromatic residue, phenylalanine, with an aliphatic group, leucine. The other substitutions (in green) are not as drastic, but also present amyloidogenic properties. Residues 18 are both basic, histidine in hIAPP and arginine in rIAPP, and residues 26 are both aliphatic, isoleucine in hIAPP and valine in rIAPP. To view the text in color, please refer the online version.

The 20–29 decapeptides of the different homologues were studied in detail with regards to their aggregation propensity, and it was shown that the S28-to-P28 substitution strongly reduced the amyloidogenecity [12]. Normally, prolines are both β-sheet and α-helix breakers, but if present as the first element in the helix, they may act as an N-capping residue and can also stabilize helices, even at higher temperatures [13,14]. Other residue substitutions, *e.g.*, rIAPP(L23F), seem to promote aggregation in rIAPP, albeit in low yield [15]. In fact, the fragment 30–37, which is identical in both homologues, aggregates *in vitro*. Hence, it is probably the overall sequence that influences the amyloidogenicity of IAPP [16].

The disulfide bond between residues C2 and C7 also plays an important role. It has been found experimentally that the presence of this disulfide bond in the peptide also changes the kinetics of aggregation, making the reaction much faster and allowing it to form fibers by secondary nucleation, leaving the structure of the IAPP fiber core intact [17].

Finding conformational differences of the two polypeptide homologues in solution could shed light on the underlying mechanism of the aggregation pathway of hIAPP and was the focus of this work using MD simulations. The properties studied in this paper were the interaction of the aromatic residues of hIAPP and rIAPP, including the mutated *in silico* variant rIAPP(L23F), the influence of the presence, or absence, of the disulfide bond in both homologues, and the effect of proline, in particular residue 28, on the secondary structure of IAPP.

2. Systems and methods

The polypeptides were modeled with MOLDEN v.4.4 [18] in an α-helical conformation and subsequently modified with SWISS-PDB VIEWER v.3.7sp5 [19]. These structures were simulated with GROMACS v.3.3.1 [20–22] using the OPLS-AA/L forcefield [23,24]. The data were analyzed by an *ad hoc* python program, which uses PYMACS v.0.2 [25] for the manipulation of the .xtc files, DSSPcont v.1.0 [26,27] and SEGNO v.3.1 [28] for the secondary structure analysis and g_sas [29] of the GROMACS package for the solvent accessible surface area. All the residues, including the termini, have been set at the standard ionization state at a pH of 7.4 at 25 °C, yielding a net charge of +3 *e* for hIAPP and +4 *e* for rIAPP. In order to neutralize the system in solution, the total charge on the biopolymer was scaled down to neutrality by distributing an equal and opposite charge on the peptide itself, as utilized by Oleinikova et al. [30].

The production runs were performed on random starting conformations, *i.e.*, conformations which were obtained after an arbitrary pre-equilibration time of at least 50 ns, and that presented a C_α RMSD of at least 1.23 nm from the initial modeled α-helix. Upon equilibration of the density of the system, these conformations were then all simulated for over 500 ns discarding at least the first 50 ns as pre-equilibration to ensure a completely random starting conformation due to the long autocorrelation times of H-bonds and secondary structure at the lower temperatures. The production isobaric-isothermal MD simulation runs of 500 ns for each moiety were performed at 1 bar at 310 K and 330 K. These MD simulations yield the temperature dependence of the radius of gyration (R_g), the end-to-end distance between C_α (r_{eted}), the maximum distance between heavy atoms (L_{max}), and the secondary structure, above and below the percolation transition [31], besides other properties like the solvent accessible surface area (SASA) and the hydrogen bonding pattern. The backbone–backbone H-bonds were identified by the following two cutoff criteria: distances between the donor (D) and the acceptor (A) atoms less than 0.35 nm and donor–hydrogen–acceptor atom angles, DHA, greater or equal to 130°. A more stringent definition, similar to the one used by Kuster et al. [32], including the carbonyl carbon of the backbone, so not only NHO is the DHA angle, but HOC is also included in the acceptance criterea, *i.e.*, both the HOC and NHO angles in NHOC must be greater than 90°, and one of the two must be greater or equal to 130°.

The peptides were solvated using equilibrated SPC/E water [33]. After proper minimization and equilibration of the system, the following 500 ns NPT production runs, in which data was collected every 2.0 ps, were performed using the Nosé–Hoover thermostat [34,35] and the Parrinello–Rahman pressure coupling [36,37] with coupling times of 2.0 ps. Constraints were applied to the water molecules by using the SETTLE [38] algorithm, while for the peptide SHAKE [39] was applied to covalent bonds involving hydrogen. Long-range electrostatic interactions were treated using the smooth particle-mesh Ewald method [40,41], with short-range interaction cutoffs set at 0.9 nm. Periodic boundary conditions were set in all three directions, with no interaction between adjacent images as the box size was set at 7 nm, the maximum distance between heavy atoms, L_{max}, being not larger than 5.5 nm.

3. Results

The most striking characteristics observed for hIAPP are the flexibility of the oxidized moiety to reach compact comformations, as opposed to rIAPP, which seems to be more rigid, possibly due to a higher helical content. The presence of the disulfide bond seems to play an important role in the initiation of the collapse of the peptide due to the stability of the threonine/disulfide interaction. The collapsed state is characterized by β-bridges and β-ladders, short tyrosine/phenylalanine distance, and a diminished hydrophobic SASA. Collapsed states are not reached by the reduced hIAPP, perhaps due to the absence of the disulfide and the presence of transient α-helices in the C-terminal region. All forms of rIAPP that have been studied seem to be too rigid to fold into conformations characterized by short r_{eted} values, which seem to be necessary for collapsing into a compact monomeric state. This rigidity seems to be caused by a pronounced helicity that includes P28.

3.1. Collapsed state of oxidized hIAPP at 330 K

The conformational properties for each moiety of hIAPP, *i.e.*, R_g, L_{max}, and SASA, increase with temperature for the cysteine moiety, as does the standard deviation of the mean, indicating a greater flexibility of the peptide with increasing temperature. At 310 K, the cystine moiety seems to be more flexible and able to explore more states that are visited by the cysteine moiety at the same temperature. A temperature dependence of such properties for the cystine moiety cannot be established without a bias, as the peptide folds into a compact state by forming β-bridges. Both moieties show a decrease in helical content with increasing temperature, while the number of H-bonds (n_{HB}) decreases with increasing temperature for the cysteine moiety, and increases for the cystine moiety. A clear anti-correlation can be observed between n_{HB} and R_g at 330 K, underlining the

compactness of the peptide. The correlation of the 100 mean values, obtained through block averages over 5 ns, is good, until the last data points, in which the R_g has reached its minimum, and the total number of H-bonds still increases (data not shown). Investigating the final portion of this simulation run, the frequency distribution of SASA (Fig. 1, bottom) shows clearly two states, one larger before the peptide folds into the compact state, and one smaller after it collapses. This can be seen not only for the total SASA (Fig. 1, in red), but in particular for the fraction of SASA relative to the hydrophobic residues (Fig. 1, in blue), hence hydrophobic interactions seem to push the peptide towards a more compact conformation.

In solution, the peptide seems to be rather compact, and although essentially random coil in nature, there are some ordered structural elements that can give additional information with regards to the aggregation propensity of the peptide. Aromatic residues, such as tyrosine and phenylalanine, seem to play an important role in the aggregation process. In the mature fibers, Y37 is close to both F15 and F23 [8], while the hIAPP peptide in solution does not have an ordered structure [5]. Measuring the distance between the C_α's of these residues at 310 K and 330 K, the average values fluctuate between 0.5 nm and 2.5 nm. This clearly shows that IAPP is more compact than what would be expected for a completely random peptide. A random walk model of the polypeptide between residues Y37/F23 and Y37/F15 predicts distances of 3.0 nm and 4.0 nm, respectively [8]. As the peptide seems unstructured in solution, we can relate the Föster distances between the tyrosine and phenylalanine to the radius of gyration. If not in the hIAPP cystine run at 330 K, there is no direct correlation between R_g and Y/F distances. Since aromatic residues that are farther than 1.8 nm apart cannot give reliable FRET results, a peptide in solution with the average distance larger than such value will be essentially unstructured. There seems to be no marked temperature dependence with this conformational property. Moreover, similar distances are found in rodent IAPP, and since F23 is not present in rIAPP, we can exclude an interaction between aromatic residues as the sole cause of stabilizing the single IAPP peptide conformation in solution. If we take the rIAPP sequence and mutate leucine into phenylalanine (L23F), which was found to form aggregates at small yields [15], there do not seem to be any significant differences in the Y37/F23 and Y37/F15 distances between the rIAPP, hIAPP, and rIAPP(L23F) moieties (data not shown). Through the data collected of the Y/F distances for oxidized hIAPP at 330 K, it is possible to shed light on the mechanism of how the peptide folds into a compact structure, as seen in Fig. 1. Since the total SASA correlates perfectly with the R_g, only the SASA data are shown. While the peptide is compact, as seen by the small SASA from 100 ns onwards (Fig. 1, top), these aromatic residues are still mobile and not buried within the peptide surface. The Y37/F23 distance fluctuates greatly from 0.4 to 2.3 nm, until it reaches the value of 1.1 nm at ~300 ns (Fig. 2a top, blue), comparable to 1.26 nm, which Padrick and Miranker measured during the lag phase in hIAPP [8]. After approximately 50 ns upon reaching this minimum, the Y37/F15 distance also reaches a minimum of ~0.8 nm (Fig. 2a top, green), presenting more fluctuations than the Y37/F23 distance. The Y37/F23 value averaged over the last 150 ns is 1.103 ± 0.002 nm and Y37/F15 is 0.86 ± 0.10 nm, which correspond to a high content of backbone–backbone H-bonds given by the β-structures (Fig. 2a bottom, green). As can be seen in Fig. 2a, the short Y37/F15 distance is necessary, but not sufficient, to fold the peptide; in fact, between 80 and 120 ns these Y/F distances are very short, but the radius of gyration is ~0.95 nm and not 0.87 nm as measured in the final 150 ns (data not shown), the former comparing nicely to the value of 0.94 nm calculated for a random-flight chain [42]. Hence, the oxidized hIAPP moiety at 330 K reaches a state, which is smaller than an unperturbed random coil, by means of interactions between aromatic residues and backbone–backbone intrapeptide H-bonds. This collapsed state of oxidized hIAPP at 330 K presents a R_g 9.0% smaller than the mean value of R_g of the 350 ns before the collapse, 11.1% smaller than the reduced moiety at 330 K, and 9.9%

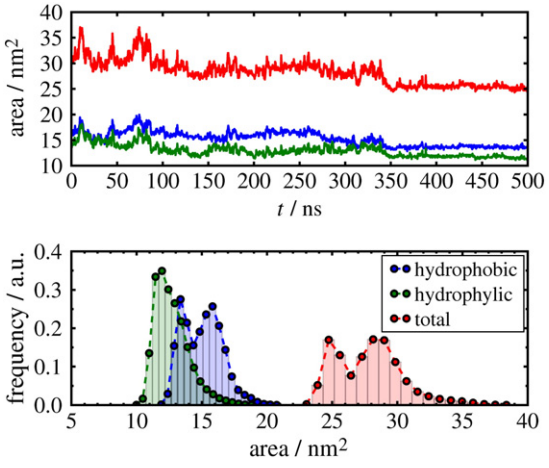

Fig. 1. Time dependence of the SASA (top) and frequency distribution of the data (bottom) of oxidized hIAPP. Hydrophopic (in blue) and total (in red) SASA both show clearly two states, while the hydrophilic SASA (in green) seems to form one single state, only.

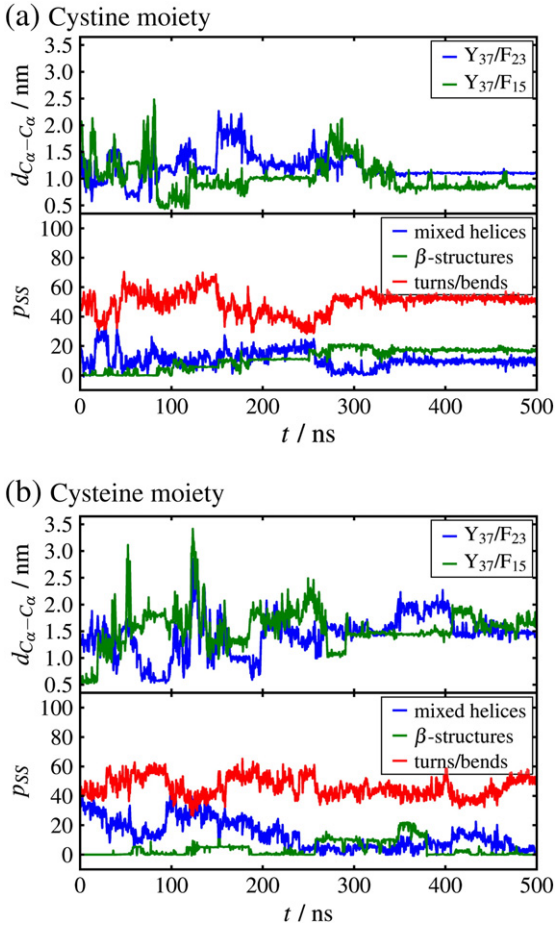

Fig. 2. Time dependence of the distance between the C_α, $d_{C\alpha-C\alpha}$, of residues Y37/F23 (in blue, top) and Y37/F15 (in green, top) and secondary structure assigned by DSSPcont (26, 27), where p_{SS} is the percentage of secondary structure elements of mixed helices (in blue, bottom), comprised collectively of 3_{10}-helices, α-helices, and π-helices, β-structures (in green, bottom), which comprise β-bridges and β-ladders, and H-bonded turns and bends (in red, bottom). The data for the two (a) cystine and (b) cysteine hIAPP moieties are plotted at 330 K.

smaller than the mean value of all the rIAPP runs at 330 K, results which agree with a higher degree of folding monomeric hIAPP found by Soong et al. [43].

Of the secondary structure assigned by DSSPcont, the β-structures, which include both β-bridges and β-ladders, show a steady increase to ~20%, starting from ~80 ns, which corresponds to the minimum Y37/F15 distance (Fig. 2a bottom, green). By comparison, the reduced moiety also presents very short Y37/F23 distances at ~80 ns (Fig. 2b top, blue), but there is no corresponding increase in β-structures (Fig. 2b bottom, green). In the same run, the β-structures do increase to ~20%, but only temporarily, and then disappear. The elevated β-structures seen in the reduced moiety correspond to larger Y/F distances (≥1.5 nm) and not ~1.1 nm as found in the oxidized moiety. Therefore, it seems, that a short Y37/F15 distance, and not Y37/F23, may initiate the folding to the observed compact state of IAPP, and both Y/F distances need to be shorter than 1.1 nm in order to stabilize it. A cluster analysis on every tenth frame of the hIAPP cystine moiety simulation run by means of the GROMOS algorithm [44] using a cutoff of 0.3 nm on the backbone atom RMSD, shows that the family of compact conformations, which includes the one stabilized by the β-structures, is present 39% of the time, *i.e.*, at least 9% more than what would be expected from 150 ns of the compact stabilized conformation. The second most populated family of structures of the first 350 ns, which is 11% of the total number of conformations, contains the centroid conformation of the most populated family of structures of the full simulation. Further investigations of the data, particularly the secondary structure and H-bonds, should allow us to shed light on this particular conformation and how it was obtained.

3.2. H-bond pattern and secondary structure of oxidized hIAPP at 330 K

The distribution of average backbone–backbone H-bonds between residues (Fig. 3) may also be used to localize secondary structure elements, by the position of H-bonds on the matrix. Such plot is defined by registering the occurrence of backbone–backbone H-bond between two residues, which are aligned along the two axes according to the peptide sequence from first to last. If the data points lie along the main diagonal, a helix may be identified. The helix, if present, may then be classified according to the number of residues between a pair, *i.e.*, four residues define an α-helix. If the data points lie perpendicular to it, such behavior is characteristic of another secondary structure, like a β-sheet.

In Fig. 3a, a detailed residue-residue H-bond matrix of the last 150 ns of the run of oxidized hIAPP at 330 K is depicted. A short helix can be seen in the N-terminus, between R11 and T4, from L16 to A13, and from N21/N22 to H18. An important point, present only in the folded peptide, is T36/C2, which also corresponds to a short r_{eted}. Other relevant points on the H-bond matrix, with occurrences above 80% (Fig. 3a, from dark blue to black) are V17/L27, F23/G33, S29/F15, N35/N21. The N21/H18 helix is present throughout the 330 K run, as are the H18/Q10 and the aforementioned β-bridges except S29/F15, albeit to a lesser extent (data for 500 ns not shown). The Ramachandran plot of the entire 500 ns run at 330 K, in comparison with the one at 310 K, shows a decreasing helical content upon heating, with increased extended conformations, in particular in the isolated β-strand region (data not shown). At 310 K, the peptide presents transient helices along the entire chain, relatively high mobility of the C-terminus, which form many H-bonds with the C-terminus half, albeit with low occurrence (data not shown). The cysteine moiety, on the other hand, shows a more prominent helical content between N22 and C2, with the C-terminal region not as mobile as seen in the oxidized counterpart at 310 K. Another persistent helical element involves T30/L27, which shifts towards S28/G24 upon heating (data not shown). At 330 K, the reduced moiety of hIAPP presents many transient helices, a flexible C-terminus, with fluctuating H-bonds

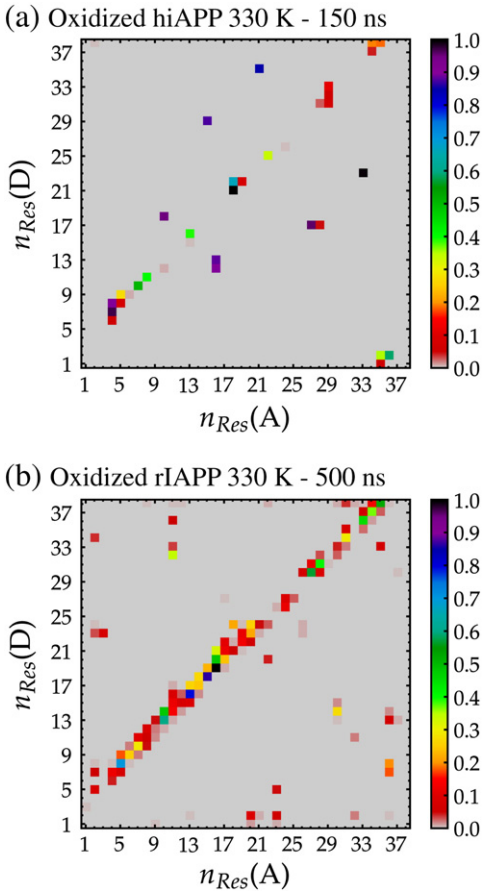

Fig. 3. Normalized distribution of the average backbone–backbone H-bond plots between residues, where the residue number, n_{Res}, on the abscissa is the acceptor (A) of the pair, and the ordinate is the donor (D). Residue 38 is the amide cap of Y37. The ROYGBIV spectral color code shows increasing occurrence while the color changes as the colors of the white light spectrum, from red to violet. The least occurence of zero is depicted in grey, and the maximum occurence is depicted in black. (a) the last 150 ns of oxidized hIAPP at 330 K; (b) 500 ns oxidized rIAPP at 330 K.

along the perpendicular diagonal, none of which corresponds to the critical points seen for the oxidized moiety (data not shown).

Fig. 3b illustrates the H-bond matrix of oxidized rIAPP at 330 K, where a strong, albeit fluctuating, helical component is found between S19 and A5, with the highest occurrence in S19/L18 and R18/F15, with none of the β-bridge elements seen for the human homologue. The C-terminal region fluctuates, but limited to transient helices, with far less points off the main diagonal as seen for the corresponding hIAPP moiety. In fact, none of the previously mentioned critical points are seen in rIAPP, especially the two H-bonds formed by H18. The H-bond matrix of rIAPP(L23F) is very similar to rIAPP, with an extremely high occurrence of helix involving N31/L27, even at 330 K. The oxidized rIAPP(L23F) mutant differs in the presence of H-bonds on the diagonal G24/N21 at 310 K and F23/S20 at 330 K (data not shown).

Intrapeptide H-bonds and consequently helical secondary structural conformations generally decrease with increasing temperature, indicating greater disordered conformations as temperature increases [45]. Interestingly enough, the helical content was more or less constant beyond 330 K, and not decreasing continuously as might be expected by comparison with the corresponding H-bond trends. This scenario might be correlated to what seems to be a quasi-2D percolation transition of the hydration water, whose midpoint is about 320 K [31,45]. In other words, the hydration water network around the peptide is more compact below 320 K and limits the

freedom of movement of the peptide, whereas above such temperature, the peptide gains flexibility and explores more easily further conformations, thus reducing the helical content of the peptide [46]. Averaging over the first 350 ns, the helical elements assigned by DSSPcont show a stark reduction upon heating for hIAPP, which correspond to an increase in β-structures, while the reduced moiety also presents increasing H-bonded turns and bends. The rIAPP data seem to be independent of the temperature increase from 310 K to 330 K (data not shown).

The time dependent plot of collective secondary structure depicted in Fig. 2 can be seen in detail in Fig. 4. hIAPP is clearly disordered in solution at 330 K, as seen in Fig. 4a, with transient 3_{10}-helices (Fig. 4a, light blue), β-bridges (Fig. 4a, violet), and β-ladders (Fig. 4a, dark blue) throughout the first 350 ns of the run. Further discussion on these particular β-ladders will be addressed in more detail later (see next subsection). At ~250 ns, the first step towards the formation of β-bridges throughout the C-terminal region occurs through a rearrangement of β-ladders (Fig. 4a, dark blue) and temporary dissolution of 3_{10}-helices (Fig. 4a, light blue), all of which occurs approximately 50 ns before the Y37/F23 distance reaches its minimum (Fig. 2a top, blue). At ~350 ns, the peptide has formed all the aforementioned β-bridges (Fig. 4a, violet) and does not change for the rest of the simulation run, presenting a helical content localized between residues A5 and T10, with the residues contributing from 32 to 82% of occurrence. The three β-bridges are all antiparallel and located as follows: A) R11/V17 and A13/L16; B) L16/S28; C) N22/S34. The definitions used to assign β-bridges in DSSPcont do not correspond to those used in the H-bond matrices, therefore the results differ slightly. However, the H-bonds calculated by UCSF Chimera [47] in the snapshot of this folded state (see Fig. 5a), correspond to the ones assigned in the H-bond matrix (Fig. 3a).

The cysteine moiety containing hIAPP at 310 K shows a transient α-helical content, localized from residues N3 to N21, and from S28 to T30, the former being disrupted by the introduction of the disulfide bond, although transient helical assignments are found in the same region. The helical content for this oxidized moiety is localized between residues A5 and V17, with the residues contributing from 6.8 to 70% of occurrence. Another transient helix is located between residues S19 and S30, with a contribution of the residues between 16 and 44%.

rIAPP shows similar trends to the corresponding human homologue (Fig. 4a), with a striking difference: rIAPP presents a more persistent helix localized near the proline residues, at L27 and N31, even at 330 K, the temperature at which a similar helix in hIAPP disappears. The H-bonding ability of residues I26 and L27, together with the flexibilty in region 25–28, have been shown to define the amyloid-forming potential of hIAPP(20–29) fragment [48,49]. Therefore, a stabile helix in this region, which limits the flexibility and the ability of forming interpeptide H-bonds, should also limit the ability to aggregate. In fact, the helical content of the cysteine moiety containing peptide disappears almost completely after ~230 ns of the

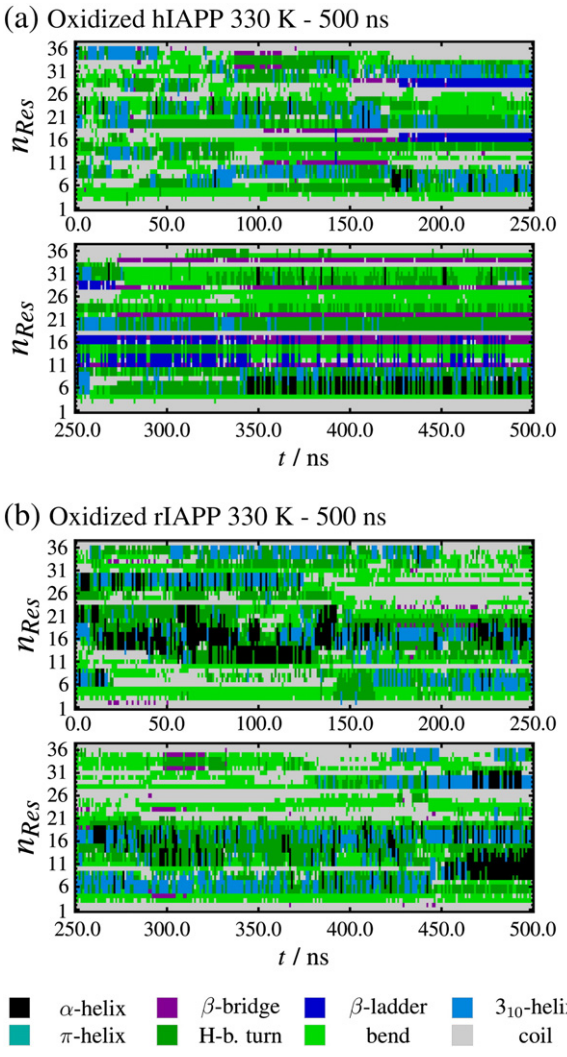

Fig. 4. Time dependence of secondary structure assigned by DSSPcont [26,27], where 3_{10}-helices are in light blue, α-helices in black, β-bridges in violet, and β-ladders in dark blue; H-bonded turns are in dark green and bends are in light green. (a) oxidized hIAPP at 330 K, and (b) oxidized rIAPP at 330 K. The data are plotted every 1.0 ns.

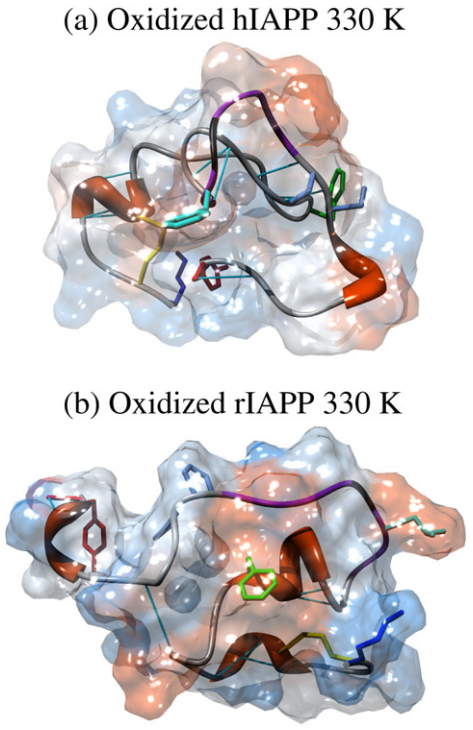

Fig. 5. Snapshots of oxidized (a) hIAPP and (b) rIAPP at 330 K, where K1 is blue, C2 and C7 are in yellow, Y37-NH2 are red, F15 is green, F23/L23 is cyan, and S28/P28 and S29/P29 are in cornflower blue. The violet ribbon corresponds to the N^{22}(F/L)GAIL^{27} sequence, with G24 in black. The POV-Ray rendered [56] images are made with UCSF Chimera [47]; the orange helices and the overall ribbon representation of the secondary structure are assigned by ksdssp [26], and the surface was calculated with the MSMS package [57]. The hydrophobicity surface shows the amino acid hydrophobicity in the Kyte-Doolittle scale [58] with colors ranging from dodger blue for the most hydrophilic to white at 0.0 to orange red for the most hydrophobic.

simulation for hIAPP and ~350 ns for rIAPP. On the other hand, the cystine moiety containing rIAPP peptide (Fig. 4b) maintains its helical content which starts from around L27, and two regions from A8 and V17. The helical content dissolves in the L27 region at ~125 ns, but reforms at ~375 ns, initially as a H-bonded turn, then as transient 3_{10}/α-helices.

The greater contribution to the helical content of the peptide of the residues 5 through 17 is characteristic to both homologues. Nanga et al. have found that the RMSD of the backbone atoms of such interval in rIAPP is 0.22 ± 0.07 Å, while the interval between 5 and 23 yields a backbone atom RMSD of 0.51 ± 0.19 Å [50]. Our calculations show a corresponding trend of smaller RMSF for residues 5–17 and larger RMSF for residues 5–23, both of which increase upon heating. The largest RMSF is found in interval 30–37, which also increases upon heating. The exception to this trend is the oxidized rIAPP at 310 K, but that seems to be due to the fact that P25 is in a *trans* conformation, which could stabilize the helicity in the otherwise more disordered C-terminus. Nanga et al. have seen that the P25 and P28, but not P29, undergo *cis–trans* isomerisation [50], but given the slowness of the *cis–trans* isomerisation [42], the transition from the initial *trans* conformation is highly unlikely during MD simulations. In the cyteine moiety rIAPP simulation, P25 underwent a *trans–cis* conformational change, and in the cystine moiety at both temperatures there are moments in which P25 presents torsion tension for another *trans–cis* isomerisation, albeit not sufficient for the transition, while P28 and P29 did not.

3.3. Flexibility and β-ladders of oxidized hIAPP at 330 K

The oxidized moiety seems to be flexible enough to fold and collapse into a compact state at temperatures above the percolation transition, *i.e.*, 320 K, while rIAPP seems too rigid to be able to fold into more compact states as also shown by Vaiana et al. [51]. It seems that also the reduced hIAPP moiety seems too rigid to fold in the central region (residues 10–20), due to the high helical content in that region; in fact the mean r_{eted} measured for all the rIAPP runs is between 1.64 nm and 2.0 nm and 1.6 ± 0.3 nm for the reduced hIAPP moiety. On the other hand, the cystine moiety reaches a very short r_{eted} of 0.54 ± 0.02 nm, confirmed by the H-bond between T36/C2 shown in Fig. 3a, which is present only for this folded peptide. This can be explained by the interaction between residues along the chain and the disulfide bond of the cystine moiety, which do not occur in the cysteine moiety [51]. There are side chain interactions with the disulfide region between T36 and both C2 and C7, albeit with an occurrence of 20–25% each. Further investigation on this compact conformation and the pathway that leads to it, shows a short antiparallel β-ladder between residues V17/S28 and L16/S29, with the residues in between forming a loop (as can be seen by the dark blue lines between ~175 ns and ~275 ns in Fig. 4a and by the H-bonds spawning from S28 and S29 in cornflower blue in Fig. 5a). This can be compared to the aggregation-prone β-hairpin conformation found by Dupuis et al. [52]. Our conformation collapses quickly into a very compact conformation, but could very well interact with neighboring peptides due to the exposure of the $N^{22}FGAIL^{27}$ (shown in Fig. 5a in violet and black ribbon), which was found along with $F^{23}GAIL^{27}$, to be the shortest sequence to form β-sheet-containing fibrils [53].

Not only helical conformations are assigned through DSSPcont, but also H-bonded turns or bends, and in such cases these prolines can induce kinks or turns, which inhibit the alignment of elements in the C-terminus necessary for β-structure formation. An example of a bend may be seen in the snapshot of rIAPP, representing the secondary structure elements, which are depicted in Fig. 5b. In Fig. 5a, a snapshot of hIAPP shows the previously discussed β-ladder seen at ~220 ns in Fig. 4a. The main element of secondary structure that can be seen is the helix in proximity of C7 (Fig. 5a, b). An exemplification of what was discussed in Fig. 2 is the distance between the C_α atoms of Y37 (in red) and F23/L23 (in cyan) and residues F15 (in green); in particular, in Fig. 5a, Y37/F15 is 1.06 nm, and Y37/F23 is 1.22 nm. The other depicted peptide presents a Y37/F15 distance of 1.6 nm, while Y37/L23 is 2.6 nm, hence leading to a compact conformation compared to random walk distances of at least 3.0 or 4.0 nm in either case.

3.4. In silico point mutations on oxidized hIAPP at 330 K

In silico mutations performed on the collapsed oxidized hIAPP conformation, S28P, S29P, and G24P, disrupt its compactness. In fact, as can be seen in Fig. 5a, S28 and S29 (side chain shown in cornflower blue), which participate in the formation of a β-sheet, and G24 (depicted by a black ribbon), whose flexibility helps in the formation of the loop between H18 and L27, would be strongly perturbed by the substitution of proline. The proline residues in the serine-to-proline single point mutations are present in rIAPP, while the glycine-to-proline is not. A short MD simulation at 330 K of the G24P mutation disrupts the secondary structure of the C-terminus, which leads to a small increase in R_g, and induces fluctuations in the Y37/F23 distances. S29P perturbs the Y37/F15 distances, from 0.87 nm to 1.02 nm and increases the radius of gyration. What is most surprising is the perturbation of the S28P mutation. It does not perturb the β-structure around it, as one might expect, rather it disrupts the end-to-end distance, most probably by inducing torsion that detaches the C-terminus from the disulfide region; in fact, the H-bond between T36/C2 shown in Fig. 3a decreases from ~60% to ~10% (data not shown). T36 then forms an H-bond with the amide terminus of Y37, with an occurrence of ~35%. Both S28P and S29P increase the mixed helical content between residues 29 to 31 from 13% to 55% and from 13% to 41%, respectively. Hence, these perturbations induced by serine-to-proline mutation, which destabilize the compact conformation in less than 10 ns of simulation, may very well be sufficient to induce rigidity in rIAPP, thus inhibiting the polypeptide to reach a short end-to-end distance, which seems necessary to reach compact states [51], or states that present aggregation-prone β-sheets [52].

4. Discussion and conclusions

Single peptide runs obviously cannot reveal mechanistic information about the aggregation process, but they can unravel conformations and regions of the peptide responsible for initiation and inhibition of the aggregation reaction of IAPP, as seen for the helix around P28, and the absence of aromatic residues in key positions like F23 in native rIAPP, and the presence or absence of the disulfide bond in hIAPP.

4.1. Compact and not entirely disordered polypeptide

Either moiety of hIAPP forms a more or less compact structure, with a small radius of gyration in either case, albeit different in secondary structure content, with the natural cystine moiety yielding a more "flexible" peptide, particularly above the percolation transition at 320 K. The oxidized moiety of hIAPP at 330 K collapses into a compact state that is about 10% smaller than both rIAPP and the reduced hIAPP moiety. The presence or absence of helical conformations, even if transient, may influence the kinetics of the aggregation. Experimental results from Koo and Miranker indicate that the aggregation is faster when the disulfide bond is present [17]. Moreover, Padrick and Miranker have shown that the aggregated peptide has an ordered C-terminus, which is less ordered when in solution [8]. Padrick and Miranker have also shown that the tyrosine and phenylalanine residues are within 1.5 nm in either homologue of IAPP [8]. The mean distance between C_α–C_α of Y37/F23 and Y37/F15 we measured, fluctuates greatly between 0.5 nm and 2.5 nm, in which many instances can be efficiently measured with FRET, thus

confirming that the peptide is not as disordered as an unfolded peptide would be with such tyrosine-phenylalanine measurable distances.

4.2. Effect of P28 on the conformation of the C-terminal region

Our MD simulations of monomeric human and rat IAPP show an important aspect of the C-terminal region which seems to be the capability of rIAPP and the *in silico* mutants hIAPP(S28P) and hIAPP (S29P) of forming helices from residue 28 on. Both rIAPP and rIAPP (L23F) form helices in this region, a region that is highly unordered in oxidized hIAPP at 330 K. This is possibly due to the nature of residue 28, one of the six different residues in sequence between human and rat IAPP. Westermark et al. have shown that the S28-for-P28 substitution inhibits the aggregation greatly [12]. Kayed et al. have shown that the polypeptides in solution are prevalently random coil in nature [5], and that is confirmed by the low content of β-structures and the transient helical content we have seen in our computer simulations.

The helical region around residue P28 is probably not the only reason why rIAPP does not aggregate, but it definitely is relevant. In fact, P28 and the ordered structure around it, could limit the interactions between the C-terminal halves of neighboring peptides, especially the H-bonding I26 and L27 residues, and the aromatic residues, which seem fundamental for the aggregation process. Thorough examination of our H-bond matrix shows that S28 is enclosed by its two neighboring residues that form pairs, V17/L27 and S29/F23, that seem to stabilize the compact conformation which presents three antiparallel β-bridges, which yield an average R_g value that is at least 9% smaller than the values calculated for the other variants of IAPP. In fact, Soong et al. have also shown that hIAPP is significantly more compact than rIAPP, suggesting a higher degree of folding [43]. Our MD simulations show a stabile helix in this region, other than bends or H-bonded turns, limiting its flexibility and the ability of forming interpeptide H-bonds, and thus should also limit its ability to aggregate.

4.3. Effect of aromatic residues

The difference in amyloidogenicity between human and rat amylin could be caused by the presence of aromatic residues along the C-terminal half. In fact, rIAPP(L23F) also aggregates, albeit at low yields [15]. However, P28 may limit the interaction of the C-terminal halves which seems relevant for interaction and aggregation. In fact, residues I26 and L27, and/or with the flexibilty in region 25–28, may define the amyloid-forming potential of the hIAPP(20–29) fragment as shown by Moriarity and Raleigh [48], and Azriel and Gazit [49].

Our *in silico* mutation of oxidized rIAPP reveals a helical region around P28 throughout the entire 500 ns MD simulation at 310 K and 330 K. Little or no secondary structure elements are located in proximity of residue F23, renders residue 23 in the oxidized L23F mutant mobile, allowing it to switch between being exposed to solvent and being imbedded within the peptide, and could therefore be able to interact with neighboring aromatic residues, thus initiating aggregate formation. Moreover, the H-bond pair F23/G33 contributing to the stability of the β-bridges, involves a phenylalanine residue, which could need Y37 to align the participating residues and initiate the formation of the β-bridges. In fact, exposure of hydrophobic patches seems to be relevant for the formation of the β-bridges, since the hydrophobic surfaces diminish with the total SASA and two clear states can be seen in the distribution of such values. Moreover, phenylalanine has been found to enhance β-sheet formation [54]. Various other elements should be considered for determining the amyloidogenicity of IAPP. The presence of P28 in rIAPP definitely influences the secondary structure of the C-terminal half. The high mobilty of F23 in rIAPP(L23F) could be the driving force of the aggregation of the L23F mutant, while the structure around P28 could be inhibiting, limiting the yield of the aggregate. Such helicity, albeit transient, may limit the mobility of residue F23, and therefore inhibit aggregate formation.

4.4. Temperature effect on oxidized hIAPP

Kayed et al. [5] have also shown that hIAPP undergoes thermal denaturation when heated from 298 K to 363 K. In particular, a highly cooperative conformational transition occurs when the temperature was raised from 308 K to 318 K, which compares well with the temperature chosen for our calculations. The percolation transition for IAPP has been calculated to be at ~320 K [31,45], so we believe studying our monomeric system at 310 K and 330 K should enable us to shed some light on the conformational transition that occurs during the lag phase prior to aggregation of hIAPP. In fact, all the runs at 310 K, with the exception of the hIAPP cystine moiety, show little or no exploration of such possible states. Moreover, at 310 K reduced hIAPP presents also a relatively stable helix starting from S28, which could be one of the causes of a slower aggregation of the cysteine moiety. On the other hand, at 330 K oxidized hIAPP is flexible enough to allow the termini to be within ~0.54 nm and form β-bridges and β-ladders in the C-terminal region, with the contemporary formation of stable, albeit transient, helices in the N-terminus, around C7. More recent studies on the temperature dependent aggregation by Vaiana et al. have shown that at lower temperatures the monomeric form could be detected for long periods of time, but aggregation appeared immediately at higher temperature [55], thus confirming the low reactivity of hIAPP at lower temperatures. Moreover, the reactive conformation of oxidized hIAPP, which was found to collapse at 330 K compared to the other relatively inert conformations that did not collapse, is confirmed by the fact that Kayed et al. [5] also found two distinct conformers that have different amyloidogenic properties, which was later confirmed by Dupuis et al. [52].

4.5. Effect of the disulfide bond

The presence of the disulfide bond in hIAPP makes the peptide more flexible and able to sample more conformations in the C-terminal half, thus facilitating interactions with neighboring peptides, as can also be seen in transient isolated β-strands localized in the C-terminus (data not shown). Moreover, the disulfide of the cystine seems to stabilize the short end-to-end distance in the oxidized moiety of hIAPP [51], allowing the formation of aggregation-prone β-sheets [52]. On the other hand, the absence of the disulfide bond also influences the stability of the peptide. In fact, the peptide shows cooperative helicity, especially at lower temperatures between residues 4 and 22, hence is less flexible, while at higher temperatures, where the turn content increases, there is no stabilizing effect of the disulfide, which forms a template to stabilize the short end-to-end distance [51], leaving the peptide completely unstructured.

Acknowledgements

The study was supported by the Deutsche Forschungsgemeinschaft, the federal state of NRW, and the IMPRS-CB in Dortmund.

References

[1] A. Kapurniotu, Amyloidogenicity and cytotoxicity of islet amyloid polypeptide, Biopolymers 60 (2001) 438–459.
[2] D.H.J. Lopes, A. Meister, A. Gohlke, A. Hauser, A. Blume, R. Winter, Mechanism of islet amyloid polypeptide fibrillation at lipid interfaces studied by infrared reflection absorption spectroscopy, Biophys. J. 93 (2007) 3132–3141.
[3] S. Jha, D. Sellin, R. Seidel, R. Winter, Amyloidogenic propensities and conformational properties of proIAPP and IAPP in the presence of lipid bilayer membranes, J. Mol. Biol. 389 (2009) 907–920.

[4] D. Sellin, L.-M. Yan, A. Kapurniotu, R. Winter, Suppression of IAPP fibrillation at anionic lipid membranes via IAPP-derived amyloid inhibitors and insulin, Biophys. Chem. 150 (2010) 73–79.
[5] R. Kayed, J. Bernhagen, N. Greenfield, K. Sweimeh, H. Brunner, W. Voelter, A. Kapurniotu, Conformational transitions of islet amyloid polypeptide (IAPP) in amyloid formation *in vitro*, J. Mol. Biol. 287 (1999) 781–796.
[6] C.E. Higham, E.T. Jaikaran, P.E. Fraser, M. Gross, A. Clark, Preparation of synthetic human islet amyloid polypeptide (iapp) in a stable conformation to enable study of conversion to amyloid-like fibrils, FEBS Lett. 470 (2000) 55–60.
[7] C. Goldsbury, K. Goldie, J. Pellaud, J. Seelig, P. Frey, S.A. Müller, J. Kistler, G.J. Cooper, U. Aebi, Amyloid fibril formation from full-length and fragments of amylin, J. Struct. Biol. 130 (2000) 352–362.
[8] S.B. Padrick, A.D. Miranker, Islet amyloid polypeptide: identification of long-range contacts and local order on the fibrillogenesis pathway, J. Mol. Biol. 308 (2001) 783–794.
[9] R. Mishra, M. Geyer, R. Winter, NMR spectroscopic investigation of early events in IAPP amyloid fibril formation, Chembiochem 10 (2009) 1769–1772.
[10] J.A. Williamson, A.D. Miranker, Direct detection of transient alpha-helical states in islet amyloid polypeptide, Protein Sci. 16 (2007) 110–117.
[11] J.D. Knight, J.A. Hebda, A.D. Miranker, Conserved and cooperative assembly of membrane-bound alpha-helical states of islet amyloid polypeptide, Biochemistry 45 (2006) 9496–9508.
[12] P. Westermark, U. Engström, K.H. Johnson, G.T. Westermark, C. Betsholtz, Islet amyloid polypeptide: pinpointing amino acid residues linked to amyloid fibril formation, Proc. Natl Acad. Sci. USA 87 (13) (1990) 5036–5040.
[13] S.C. Li, N.K. Goto, K.A. Williams, C.M. Deber, Alpha-helical, but not beta-sheet, propensity of proline is determined by peptide environment, Proc. Natl Acad. Sci. USA 93 (1996) 6676–6681.
[14] J.S. Richardson, D.C. Richardson, Amino acid preferences for specific locations at the ends of alpha helices, Science 240 (1988) 1648–1652.
[15] J. Green, C. Goldsbury, T. Mini, S. Sunderji, P. Frey, J. Kistler, G. Cooper, U. Aebi, Full-length rat amylin forms fibrils following substitution of single residues from human amylin, J. Mol. Biol. 326 (2003) 1147–1156.
[16] M.R. Nilsson, D.P. Raleigh, Analysis of amylin cleavage products provides new insights into the amyloidogenic region of human amylin, J. Mol. Biol. 294 (1999) 1375–1385.
[17] B.W. Koo, A.D. Miranker, Contribution of the intrinsic disulfide to the assembly mechanism of islet amyloid, Protein Sci. 14 (2005) 231–239.
[18] G. Schaftenaar, J. Noordik, Molden: a pre- and post-processing program for molecular and electronic structures, J. Comput.-Aided Mol. Des. 14 (2000) 123–134.
[19] N. Guex, M. Peitsch, SWISS-MODEL and the Swiss-PdbViewer: an environment for comparative protein modeling, Electrophoresis 18 (1997) 2714–2723. http://www.expasy.org/spdbv/.
[20] E. Lindahl, B. Hess, D. van der Spoel, Gromacs 3.0: a package for molecular simulation and trajectory analysis, J. Mol. Model. 7 (2001) 306–317.
[21] H.J.C. Berendsen, D. van der Spoel, R. van Drunen, Gromacs: a message-passing parallel molecular dynamics implementation, Comp. Phys. Comm. 91 (1995) 43–56.
[22] D. van der Spoel, E. Lindahl, B. Hess, G. Groenhof, A. Mark, H.J.C. Berendsen, Gromacs: fast, flexible and free, J. Comput. Chem. 26 (2005) 1701–1719.
[23] W.L. Jorgensen, J. Tirado-Rives, The OPLS [optimized potentials for liquid simulations] potential functions for proteins, energy minimizations for crystals of cyclic peptides and crambin, J. Am. Chem. Soc. 110 (1988) 1657–1666.
[24] G. Kaminski, R. Friesner, J. Tirado-Rives, W. Jorgensen, Evaluation and reparametrization of the OPLS-AA force field for proteins via comparison with accurate quantum chemical calculations on peptides, J. Phys. Chem. B 105 (2001) 6474–6487.
[25] D. Seeliger, Python/Gromacs Interface, http://wwwuser.gwdg.de/~dseelig/pymacs.html2004.
[26] W. Kabsch, C. Sander, Dictionary of protein secondary structure: pattern recognition of hydrogen-bonded and geometrical features, Biopolymers 22 (1983) 2577–2637.
[27] C.A.F. Andersen, A.G. Palmer, S. Brunak, B. Rost, Continuum secondary structure captures protein flexibility, Structure 10 (2002) 175–184.
[28] M.V. Cubellis, F. Cailliez, S.C. Lovell, Secondary structure assignment that accurately reflects physical and evolutionary characteristics, BMC Bioinform. 6 (Suppl 4) (2005) S8.
[29] D. Eisenberg, A. McLachlan, Solvation energy in protein folding and binding, Nature 319 (1986) 199–203.
[30] A. Oleinikova, N. Smolin, I. Brovchenko, A. Geiger, R. Winter, Formation of spanning water networks on protein surfaces via 2D percolation transition, J. Phys. Chem. B 109 (2005) 1988–1998.
[31] I. Brovchenko, M.N. Andrews, A. Oleinikova, Volumetric properties of human islet amyloid polypeptide in liquid water, Phys. Chem. Chem. Phys. 12 (2010) 4233–4238.
[32] D.J. Kuster, S. Urahata, J.W. Ponder, G.R. Marshall, From data or dogma? The myth of the ideal helix, Biophys. J. 96 (2009) 5a.
[33] H.J.C. Berendsen, J.R. Grigera, T.P. Straatsma, The missing term in effective pair potentials, J. Phys. Chem. 91 (1987) 6269–6271.
[34] S. Nosé, A molecular dynamics method for simulations in the canonical ensemble, Mol. Phys. 52 (1984) 255–268.
[35] W. Hoover, Canonical dynamics: equilibrium phase-space distributions, Phys. Rev. A 31 (1985) 1695–1697.
[36] M. Parrinello, A. Rahman, Polymorphic transitions in single crystals: a new molecular dynamics method, J. Appl. Phys. 52 (1981) 7182–7190.
[37] S. Nosé, M. Klein, Constant pressure molecular dynamics for molecular systems, Mol. Phys. 50 (1983) 1055–1076.
[38] S. Miyamoto, P. Kollman, SETTLE: an analytical version of the SHAKE and RATTLE algorithims for rigid water models, J. Comput. Chem. 12 (1992) 952–962.
[39] J. Ryckaert, G. Ciccotti, H.J.C. Berendsen, Numerical integration of the cartesian equations of motion of a system with constraints; molecular dynamics of n-alkanes, J. Comput. Phys. 23 (1977) 327–341.
[40] T. Darden, D. York, L. Pedersen, Particle mesh ewald: an N-log(N) method for ewald sums in large systems, J. Chem. Phys. 98 (1993) 1311–1327.
[41] U. Essmann, L. Perera, M.L. Berkowitz, T. Darden, H. Lee, L.G. Pedersen, A smooth particle mesh ewald method, J. Chem. Phys. 103 (1995) 8577–8593.
[42] T.E. Creighton, Proteins: Structure and Molecular Properties, 2nd EditionW. H. Freeman and Company, New York, 1993.
[43] R. Soong, J.R. Brender, P.M. Macdonald, A. Ramamoorthy, Association of highly compact type II diabetes related islet amyloid polypeptide intermediate species at physiological temperature revealed by diffusion NMR spectroscopy, J. Am. Chem. Soc. 131 (2009) 7079–7085.
[44] X. Daura, K. Gademann, J. Bernhard, D. Seebach, W.F. van Gunsteren, A.E. Mark, Peptide folding: when simulation meets experiment, Angew. Chem. Int. Ed Engl. 38 (1999) 236–240.
[45] U.H.E. Hansmann, J.H. Meinke, S. Mohanty, W. Nadler, O. Zimmermann (Eds.), From Computational Biophysics to Systems Biology (CBSB08), NIC series, NIC-Directors, 40, 2008. http://www.fz-juelich.de/nic-series/volume40/volume40.html.
[46] I. Brovchenko, A. Oleinikova, Which properties of a spanning network of hydration water enable biological functions? Chemphyschem 9 (2008) 2695–2702.
[47] E.F. Pettersen, T.D. Goddard, C.C. Huang, G.S. Couch, D.M. Greenblatt, E.C. Meng, T.E. Ferrin, UCSF chimera—a visualization system for exploratory research and analysis, J. Comput. Chem. 25 (2004) 1605–1612.
[48] D.F. Moriarty, D.P. Raleigh, Effects of sequential proline substitutions on amyloid formation by human amylin 20–29, Biochemistry 38 (1999) 1811–1818.
[49] R. Azriel, E. Gazit, Analysis of the minimal amyloid-forming fragment of the islet amyloid polypeptide. An experimental support for the key role of the phenylalanine residue in amyloid formation, J. Biol. Chem. 276 (2001) 34156–34161.
[50] R.P.R. Nanga, J.R. Brender, J. Xu, K. Hartman, V. Subramanian, A. Ramamoorthy, Three-dimensional structure and orientation of rat islet amyloid polypeptide protein in a membrane environment by solution nmr spectroscopy, J. Am. Chem. Soc. 131 (2009) 8252–8261.
[51] S.M. Vaiana, R.B. Best, W.-M. Yau, W.A. Eaton, J. Hofrichter, Evidence for a partially structured state of the amylin monomer, Biophys. J. 97 (2009) 2948–2957.
[52] N.F. Dupuis, C. Wu, J.-E. Shea, M.T. Bowers, Human islet amyloid polypeptide monomers form ordered beta-hairpins: a possible direct amyloidogenic precursor, J. Am. Chem. Soc. 131 (2009) 18283–18292.
[53] K. Tenidis, M. Waldner, J. Bernhagen, W. Fischle, M. Bergmann, M. Weber, M.L. Merkle, W. Voelter, H. Brunner, A. Kapurniotu, Identification of a penta- and hexapeptide of islet amyloid polypeptide (IAPP) with amyloidogenic and cytotoxic properties, J. Mol. Biol. 295 (2000) 1055–1071.
[54] T. Schlick, Molecular Modeling and Simulation: An Interdisciplinary Guide, Springer, New York, 2006.
[55] S.M. Vaiana, R. Ghirlando, W.-M. Yau, W.A. Eaton, J. Hofrichter, Sedimentation studies on human amylin fail to detect low-molecular-weight oligomers, Biophys. J. 94 (2008) L45–L47.
[56] Persistence of Vision Pty. Ltd., Persistence of Vision (TM) Raytracer, Persistence of Vision Pty. Ltd, Williamstown, Victoria, Australia, 2004, http://www.povray.org/.
[57] M.F. Sanner, A.J. Olson, J.C. Spehner, Reduced surface: an efficient way to compute molecular surfaces, Biopolymers 38 (1996) 305–320.
[58] J. Kyte, R. Doolittle, A simple method for displaying the hydropathic character of a protein, J. Mol. Biol. 157 (1982) 105–132.